Interference effect in low-order harmonic generation of H_2^+ in intense laser fields

Ling-Ling Du, Guo-Li Wang,* Peng-Cheng Li, and Xiao-Xin Zhou†
Key Laboratory of Atomic and Molecular Physics and Functional Materials of Gansu Province, College of Physics and Electronic Engineering, Northwest Normal University, Lanzhou 730070, China

Zeng-Xiu Zhao‡
Department of Physics, National University of Defense Technology, Changsha 410073, China

(Received 20 December 2017; published 2 February 2018)

We explore the mechanism of the low-order harmonic generation (LOHG) of hydrogen molecular ions in an intense laser field by solving three-dimensional time-dependent Schrödinger equation. Our simulations show that the LOHG of hydrogen molecular ions at large internuclear distances exhibits spectral and temporal fine subpeak structures. Combining with a two-state model and the Morlet transform, the dynamical origin of the LOHG is clarified. We find that the interference in cycles of the multiphoton radiation during the dipole transition between the ground state and the first excited state results in the generation of the spectral subpeak structures. Our results contribute to better understanding of the generation of low-order harmonics.

DOI: 10.1103/PhysRevA.97.023404

I. INTRODUCTION

The high-order harmonic generation (HHG), resulted from the interaction of strong laser field with atoms, ions, and molecules, is an important radiation source. In the past decades, the HHG at the plateau and near the cutoff region has attracted considerable attention due to their potential applications, such as attosecond time-resolved spectroscopy [1,2], observation and control of the electronic dynamical behaviors in attosecond time scale [3–12], etc. More recently, the low-order harmonic generation (LOHG) has been the new research focus owing to its applications as a high-repetition-rate and high-intensity light source; thus some pioneering works have been carried out both theoretically and experimentally [13–18].For instance, Li *et al.* [19] studied the dynamical origin of below-threshold harmonic generation of Cs atom. Xiong *et al.* [20] observed the new below-threshold harmonics when the electron from atom was ionized from the excited states and recombined to the ground state. Heslar *et al.* [21] found that the effects of multirescattering trajectories gradually disappeared in the below-threshold harmonic generation process from diatomic molecule H_2^+. For very low-order harmonics, the only study of Avanaki *et al.* [22] observed that the 3rd, 5th, and 7th harmonics were split in double peaks due to the resonance between the ground $1\sigma_g$ and the first excited $1\sigma_u$ state. However, the dynamical origin of such low-order harmonic generation for molecular systems is yet understood and largely unexplored.

In this work, we focus on this important issue by studying the LOHG of the homonuclear diatomic molecule H_2^+. We find that the 3rd, 5th, and 7th harmonics present the fine subpeak structures at the larger internuclear distances. We interpret these fine structures as the effects of the interferences [23,24] of the multiphoton radiation in different cycles during the dipole transition between the ground and the first excited states. Under some specific conditions, these fine subpeak structures can also be found at small internuclear distances.

The article is organized as follows. In Sec. II, we mainly introduce the theoretical framework. In Sec. III, the results and discussions of the LOHG in hydrogen molecular ions are presented. Conclusions are given in Sec. IV.

II. THEORETICAL METHODS

We assume the molecular axis of H_2^+ is directed along the z axis and the two nucleuses are located on this axis at the positions of $-a$ and a, respectively; thus the internuclear distance $R = 2a$. The harmonic spectrum for a molecular target generated by a linearly polarized laser field can be calculated by solving the three-dimensional time-dependent Schrödinger equation (3D TDSE) within the prolate spheroidal coordinate (ξ,η,φ), which is related to the Cartesian coordinate (x,y,z) as follows [25,26]:

$$\begin{aligned} x &= a\sqrt{(\xi^2-1)(1-\eta^2)}\cos(\varphi), \\ y &= a\sqrt{(\xi^2-1)(1-\eta^2)}\sin(\varphi), \\ z &= a\xi\eta. \end{aligned} \tag{1}$$

At first, we solve the time-independent Schrödinger equation to obtain the ground-state wave function

$$H_0\Psi(\xi,\eta,\varphi) = E\Psi(\xi,\eta,\varphi), \tag{2}$$

where $H_0 = -\frac{1}{2}\nabla^2 + V(\xi,\eta)$ is the unperturbed electronic Hamiltonian which includes the kinetic energy and the Coulomb interactions with the two nuclei. The Laplacian operator and the Coulomb interactions are as follows (the

*Corresponding author: wanggl@nwnu.edu.cn
†Corresponding author: zhouxx@nwnu.edu.cn
‡Corresponding author: zhao.zengxiu@gmail.com

charge of each nuclear is unity for H_2^+):

$$\nabla^2 = \frac{1}{a^2(\xi^2-\eta^2)}\left[\frac{\partial}{\partial\xi}(\xi^2-1)\frac{\partial}{\partial\xi} + \frac{\partial}{\partial\eta}(\eta^2-1)\frac{\partial}{\partial\eta} + \frac{\xi^2-\eta^2}{(\xi^2-1)(1-\eta^2)}\frac{\partial^2}{\partial^2\varphi}\right], \tag{3}$$

$$V(\xi,\eta) = -\frac{2\xi}{a(\xi^2-\eta^2)}. \tag{4}$$

The wave function $\Psi(\xi,\eta,\varphi)$ is expanded by a Fourier series with respect to the angular coordinate,

$$\Psi(\xi,\eta,\varphi) = \sum_m \Psi^m(\xi,\eta)\frac{e^{im\varphi}}{\sqrt{2\pi}}. \tag{5}$$

We expand the wave function $\Psi^m(\xi,\eta)$ in a product basis of discrete-variable-representation (DVR) functions,

$$\Psi^m(\xi,\eta) = \sum_{i,j} c^m_{i,j} f_i(\xi) g_j(\eta). \tag{6}$$

The more detailed numerical procedures can be found in Refs. [25–27].

Once the initial wave function is available, we discretize and propagate the time-dependent wave function in the laser field by means of the second-order split-operator method [28], which reads

$$\Psi(t+\Delta t) = \exp\left(-i\frac{\Delta t}{2}H_0\right)\exp\left[-i\Delta t U\left(t+\frac{\Delta t}{2}\right)\right] \times \exp\left(-i\frac{\Delta t}{2}H_0\right)\Psi(t) + O[(\Delta t)^3]. \tag{7}$$

In Eq. (7), the interaction potential with a linearly polarized laser field is given as

$$U(\xi,\eta,\varphi,t) = aE(t)[\sqrt{(\xi^2-1)(1-\eta^2)}\cos(\varphi) \times \sin(\theta) + \xi\eta\cos(\theta)]. \tag{8}$$

Here θ is the angle between the polarization vector of the laser field and the molecular axis and $E(t)$ is the electric field of laser pulse.

The spectra density of the harmonic radiation can be calculated in the length form

$$S(\omega) = \frac{2\omega^4}{3\pi c^3}|d(\omega)|^2 \tag{9}$$

and in the acceleration form

$$S(\omega) = \frac{2}{3\pi c^3}|a(\omega)|^2. \tag{10}$$

Here, $d(\omega)$ and $a(\omega)$ are the Fourier transforms of the time-dependent dipole moment in the length form and acceleration form, respectively,

$$d(t) = \langle\Psi(t)|z|\Psi(t)\rangle, \tag{11}$$

$$a(t) = \langle\Psi(t)|-\frac{\partial V}{\partial z} - eE(t)|\Psi(t)\rangle. \tag{12}$$

The length and acceleration forms provide almost identical results for HHG spectra, indicating a full convergence of our wave functions.

In addition, we perform the time-frequency analysis on the induced dipole moment of H_2^+ with the Morlet transform [24,29,30] to probe the features of the HHG. The form of the Morlet transform is given by

$$A_\omega(t_0,\omega) = \int a(t) w_{t_0,\omega} dt = A_\omega(t_0), \tag{13}$$

where

$$w_{t_0,\omega} = \sqrt{\omega} W[\omega(t-t_0)], \tag{14}$$

$$W(x) = \frac{1}{\tau}e^{ix}e^{-x^2/2\tau^2}. \tag{15}$$

Here, we choose the window width parameter $\tau = 15$ in the time-frequency analysis.

III. RESULTS AND DISCUSSION

In our simulations, the linear polarized electric field $E(t)$ with a Gaussian-shape pulse envelope is given as $E(t) = E_0 e^{-2\ln 2(t^2/\tau^2)}\sin(\omega t)$, where the central wavelength is 1064 nm, the duration is 30 optical cycles (the full width at half maximum pulse duration is about 18 fs), and the laser peak intensity is 1×10^{14} W/cm^2.

In Figs. 1(a) and 1(b), we show the calculated power spectra of H_2^+ for the two internuclear distances, that is, $R = 2$ a.u. (the equilibrium internuclear distance) and $R = 7$ a.u., respectively. According to the atomic recollision model [31], the cutoff of the harmonics is located at the energy of $I_p + 3.17U_p$, where $U_p = E_0^2/4\omega^2$ is the ponderomotive energy and I_p is the ionization energy of the initial state. In our case the vertical ionization energies of H_2^+ at the two internuclear distances are 1.10 a.u. and 0.65 a.u., respectively, corresponding to the cutoff harmonic orders of 54 and 43, which agrees well with the

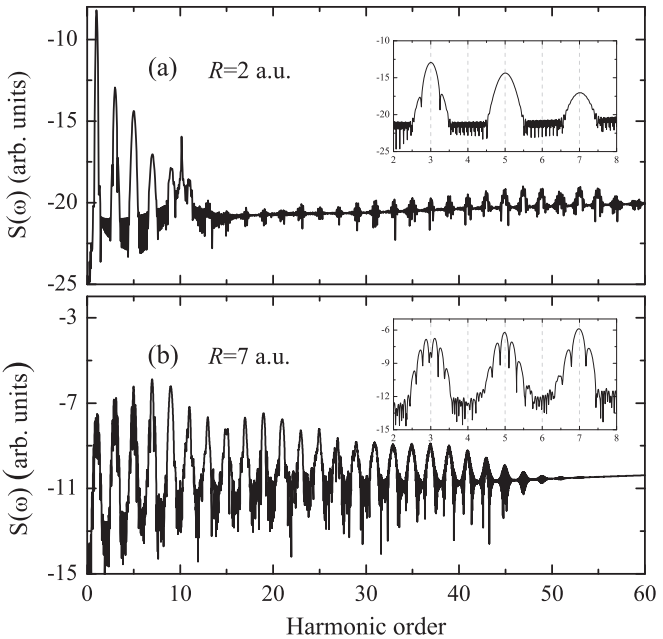

FIG. 1. Power spectra of H_2^+ driven by a 1064-nm laser pulse with the peak intensity of 1×10^{14} W/cm^2 for internuclear distance of (a) $R = 2$ a.u. and (b) $R = 7$ a.u., respectively.

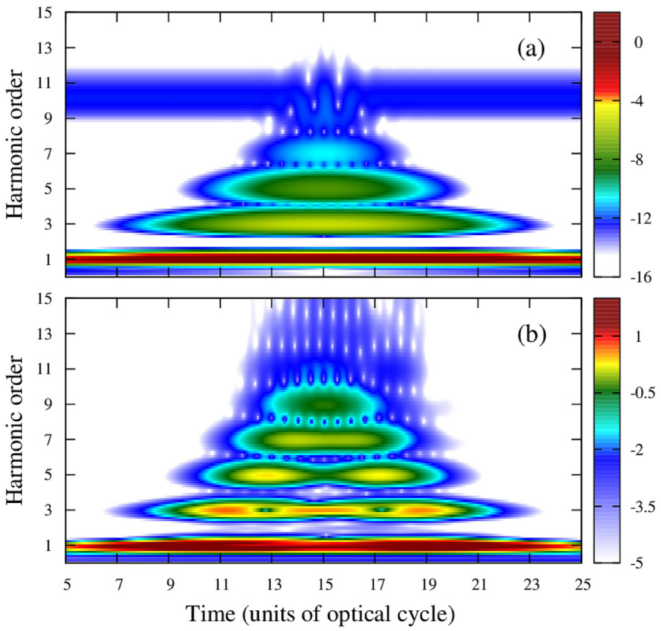

FIG. 2. Wavelet time-frequency spectra of the dipole moment along the molecular axis (z direction). The parameters used are the same as those in Fig. 1.

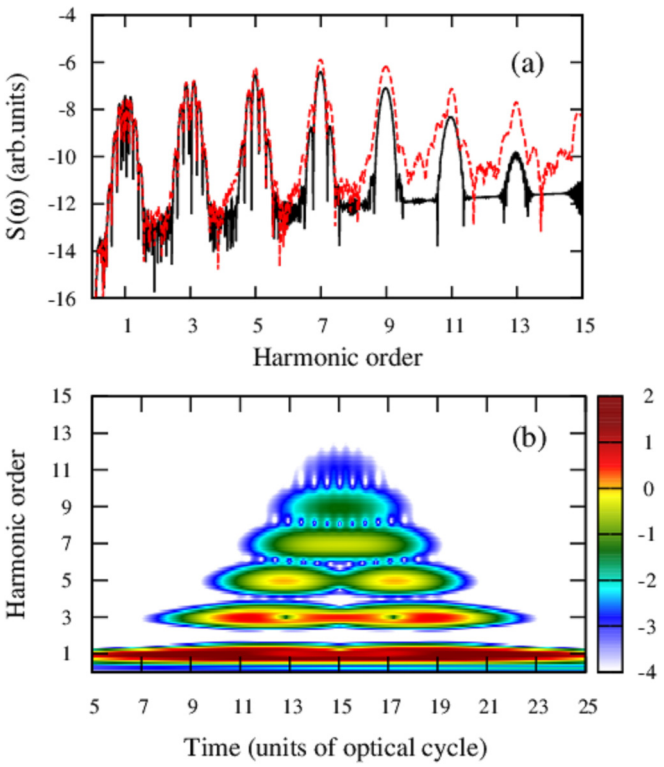

FIG. 3. (a) Comparison of the power spectra of H_2^+ obtained from simulations of TDSE (red dash line) and two-state model (black solid line). The internuclear distance is 7 a.u. (b) The corresponding wavelet time-frequency spectrum calculated using two-states model.

TDSE simulations. It is also shown that the harmonic intensity at the small internuclear distance is much lower than those of the large internuclear distance, owing to small ionization probability. More importantly, from the comparison of the enlarged low-order harmonic spectra shown in the inset, we can see that, unlike the case of small R, the spectra around the 3rd, 5th, and 7th harmonics present some subpeak structures for the $R = 7$ a.u. (the first-order harmonics contained laser energy is not considered here). We note that the similar results are also found in Ref. [22]; however, the reasons for these subpeak structures are not discussed in detail there.

Figures 2(a) and 2(b) present the wavelet time-frequency spectra of H_2^+ with internuclear distances of 2 a.u. and 7 a.u., respectively. As expected, the harmonics are generated mainly during the central part of the laser pulse. At $R = 2$ a.u., one can see a strong line close to the 10th harmonic, which always exists due to the resonance transition between the ground state $1\sigma_g$ and first excited state $1\sigma_u$ with Stark shift. For $R = 7$ a.u., along the emission of the 3rd and 5th harmonics, some unusual minima show up. It is expected that different mechanisms of harmonic radiation may be responsible for these subpeak structures at $R = 7$ a.u. More discussions about these will be presented later.

To interpret the LOHG of H_2^+ with a large internuclear distance, Avanaki *et al.* [22] pointed out that the ground $1\sigma_g$ and first excited $1\sigma_u$ states (abbreviated as $|g\rangle$ and $|u\rangle$) are two charge resonance states that are strongly coupled with each other by radiative interaction. Thus it is justified to reproduce the low-order harmonics by using the simple two-state model in terms of the states $|g\rangle$ and $|u\rangle$ [32–34]. Although this model cannot directly take the ionization process into account, it can help to understand the radiation processes of the LOHG. In this model, at first, a population transitions from the field-dressed state $|\phi_1\rangle$ to the state $|\phi_2\rangle$, then the system gains energy from the field, and finally the population transitions from $|\phi_2\rangle$ back to $|\phi_1\rangle$ with the energy released in the form of harmonic radiation. Within this picture, the time-dependent wave function is given by

$$\phi_1 = \cos(\theta_1)|g\rangle + \sin(\theta_1)|u\rangle, \tag{16}$$

$$\phi_2 = -\sin(\theta_1)|g\rangle + \cos(\theta_1)|u\rangle, \tag{17}$$

where

$$\theta_1 = -\frac{1}{2}\arctan\left[\frac{2H_{gu}E(t)}{\Delta\varepsilon_{gu}}\right], \tag{18}$$

with dipole matrix element $H_{gu} = \langle g|z|u\rangle$ and energy separation $\Delta\varepsilon_{gu} = \varepsilon_u - \varepsilon_g$. The field-dressed eigenvalues can be obtained as

$$\varepsilon_{1,2}(t) = \tfrac{1}{2}[\varepsilon_u + \varepsilon_g \mp \sqrt{\Delta\varepsilon_{gu}^2 + 4|H_{gu}E(t)|^2}]. \tag{19}$$

Then, the harmonic spectrum can be obtained from Eqs. (9) or (10).

We simulate LOHG using the two-state model and compare the spectra with TDSE simulations in Fig. 3(a), for $R = 7$ a.u. As shown in the figure, the structure of the low-order harmonics from the two-states model agrees well with that calculated by the TDSE, which indicates the electric dipole transition from the two field-dressed states is very significant for the LOHG. Thus it is reasonable to apply this model to demonstrate the origin of the subpeak structures around low-order harmonics. In Fig. 3(b), we show the wavelet time-frequency spectrum

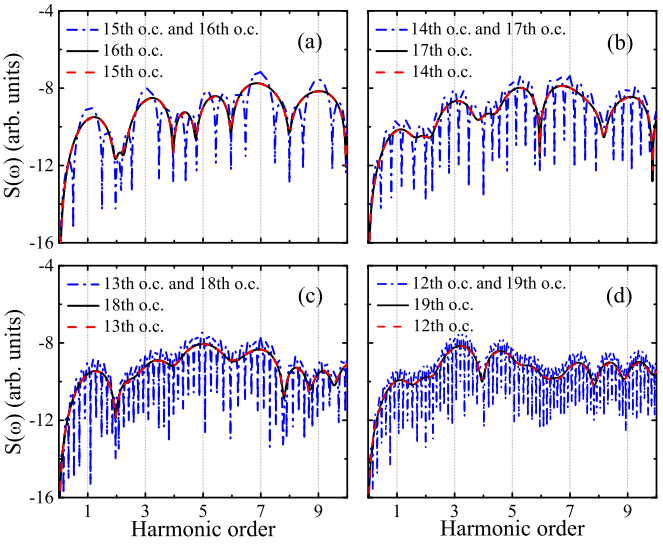

FIG. 4. Interferences of harmonic emissions from antisymmetric (a) 15th and 16th, (b) 14th and 17th, (c) 13th and 18th, and (d) 12th and 19th optical cycles of laser pulse, respectively. The black solid and red dash lines present the power spectra generated in given a single optical cycle of laser pulse and blue dash-dot line is the superposition of them.

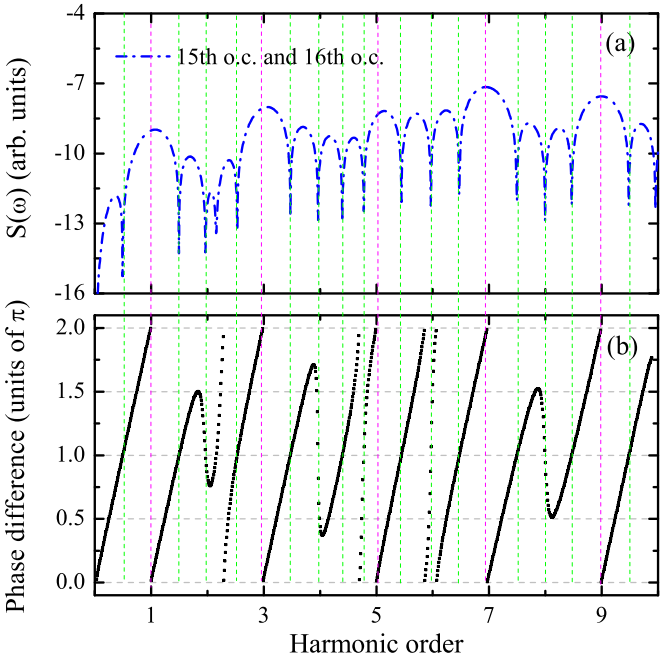

FIG. 5. (a) Superposed power spectrum of harmonics generated in the 15th and 16th optical cycles of laser pulse. (b) The corresponding harmonic phase difference. The vertical dashed magenta and green lines refer to the constructive and destructive interferences, respectively.

calculated from the two-state model. It proves again the consistency between two methods. The harmonic emission time in the two-states model coincides exactly with that in TDSE calculations shown in Fig. 2(b). The higher the frequency, the narrower the emission time interval is. The 3rd, 5th, and 7th harmonics are generated mainly during 11–20, 12–19, and 14–17 optical cycles of laser pulse, respectively. Besides, the simulations also show two and one minima in the emission of the 3rd and 5th harmonics [see Fig. 3(b)], respectively.

To explore the subpeaks of low-order harmonics, we calculate the power spectra generated within an individual optical cycle of the laser pulse using the two-state model, and then superpose coherently two of them. To see the most obvious interferences, two antisymmetric cycles are chosen. From the results shown in Fig. 4, we can see that spectrum generated in a single optical cycle displays ordinary structure. After superposition, many fine peaks appear. This indicates that the subharmonics in Fig. 1 may come from the interferences of the dipole transition radiation emitted from the two lowest bound states within different optical cycles.

We further calculate the phase difference $\Delta\psi$ of harmonics generated in two antisymmetric optical cycles. Figure 5 shows an example for the 15th and 16th cycles. For reference, the superposed harmonic spectrum is also shown. For the integral odd (1st, 3rd, 5th, ...) harmonics from two cycles, they are in phase ($\Delta\psi = 2k\pi$, $k = 0,1,\ldots$), these radiation are enhanced due to constructive interferences. While the integral even (0th, 2nd, 4th, ...) and half (0.5th, 1.5th, 2.5th, ...) harmonics are out of phase [$\Delta\psi = (2k+1)\pi, k = 0,1,\ldots$], destructive interferences result in minima at these frequencies.

In order to produce the entire spectrum, more cycles need to be included. Figure 6 shows the evolution of power spectra with a number of optical cycles included in the calculation of the dipole moment. We can see that the interferences produce well all fine structures around main harmonics with more cycles. These results indicate that all the harmonic subpeaks are produced by the same mechanism, namely, they are produced by the interferences in cycles of all the multiphoton radiation emitted from the dipole transition of the two lowest bound

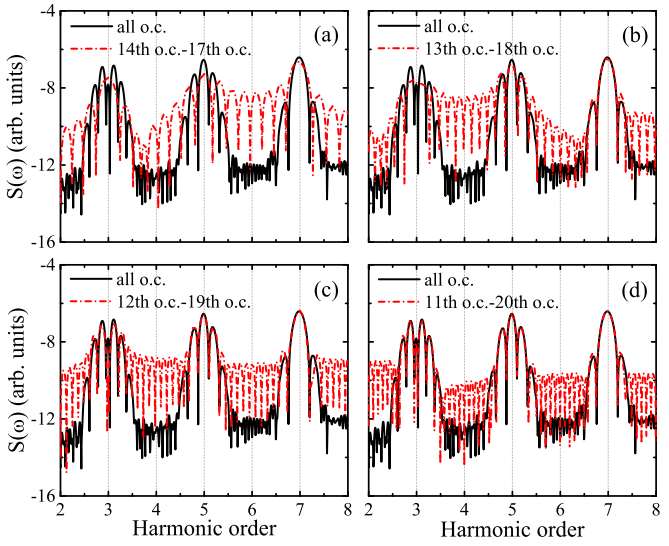

FIG. 6. Evolution of the power spectra with a number of optical cycles included in the calculation of dipole moment.

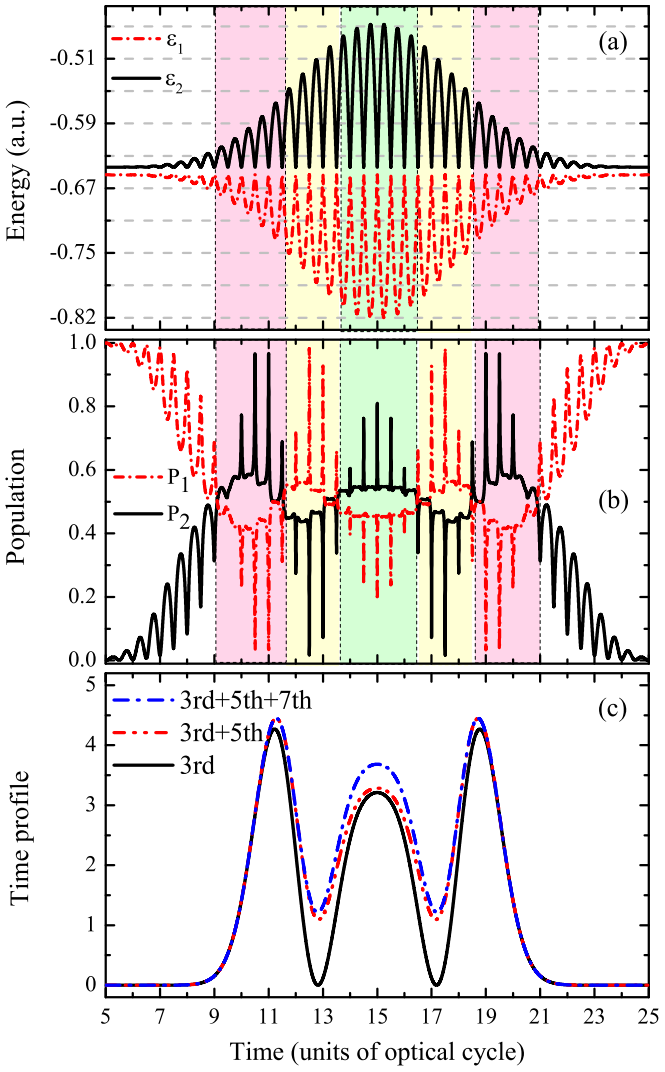

FIG. 7. Function of (a) field-dressed energies $\varepsilon_1(t)$ (red-dash-dot line), $\varepsilon_2(t)$ (black-solid line) and (b) the populations P_1 (red dash-dot line), P_2 (black solid line) for the $|\phi_1\rangle$ and $|\phi_2\rangle$ states with time. The energy difference between the two neighboring gray dashed lines equals ω. (c) The time profile of the 3rd (black solid line), 5th (red dash-dot-dot line), and 7th (blue dash-dot line) harmonics.

states within the incident laser pulse duration. Our results further confirm the prediction of the Protopapas model [23] for the harmonic emission.

To understand the two minima in the emission of the 3rd harmonic, we turn to the time-dependent energy and population of two states. Figures 7(a) and 7(b) show the evolution of the field-dressed energies $\varepsilon_{1,2}(t)$ and population transition with emission time for the internuclear distance $R = 7$ a.u., and Fig. 7(c) depicts the time profiles of the 3rd, 5th, and 7th harmonics. According to the emission frequency (1st harmonic not considered here) and relationship of population of two states, we partition the whole emission to five periods (as shown by shadow regions in the figure). In each period the number of emitted harmonics is different and the populations for two states vary around 50%. For the 1st and 5th periods, the population of the excited state P_2 has the biggest value and has the relation of $P_2 > P_1$, so the only emitted 3rd harmonic has

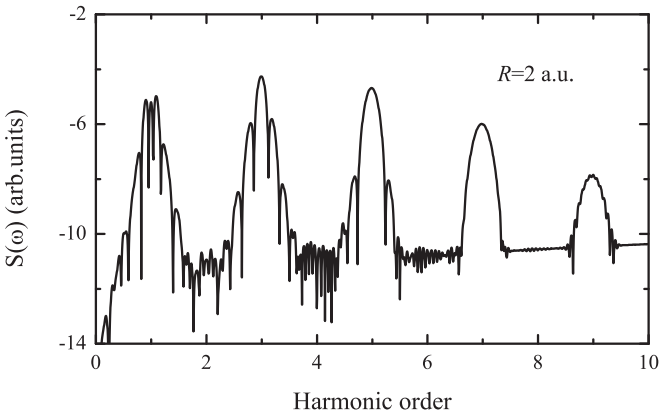

FIG. 8. LOHG of H_2^+ with internuclear distances of 2 a.u. The wavelength and peak intensity are 45 nm and 1×10^{17} W/cm^2, respectively.

the strongest intensity. In the 2nd and 4th periods, in view of the energy, two harmonic frequencies (3rd and 5th) would be emitted. Furthermore, the total strength of these two harmonics should be smaller than those in the 1st and 5th periods due to $P_2 < P_1$. Thus two minima appear for the 3rd harmonic emission. It is worth noting that in this case P_2 yet has a nonzero value of about 45%, so the strong 5th harmonic is still emitted. In the 3rd period, $P_2 > P_1$, and three (3rd, 5th, 7th) harmonics would be emitted. Similarly, the 3rd and 5th harmonic radiations are weaker than those generated in other periods.

As one can see in Fig. 2 and Fig. 7(c), the time profiles of the 3rd, 5th, and 7th harmonics in the equilibrium internuclear distance are analogous to the laser field envelope, while the results in the larger internuclear distance show interesting fine structures of the time profiles of the LOHG due to changes of physical origin. Indeed, our discussion above for these fine structures provides a good understanding for the LOHG in the larger internuclear distance. On the other hand, these subpeak structures of the LOHG in the larger internuclear distance are changed when the effect of nuclear vibration is considered, such as the peak shift and the changes of harmonic radiation intensity [35–37], but the whole subpeak structures of the LOHG in the larger internuclear distance still exist.

Lastly, we recalculate the LOHG of H_2^+ at internuclear distance $R = 2$ a.u. with a set of new laser parameters using the two-state model. In the calculation, the wavelength and peak intensity are 45 nm and 1×10^{17} W/cm^2, respectively (the Keldysh parameter γ is close to that used for $R = 7$ a.u.). One can see from Fig. 8 that there also exhibit similar subpeak structures in the low-order region in this case. Therefore, to observe the interferences in the LOHG process, it is crucial to choose an appropriate laser frequency, which is comparable with the energy difference between the ground state and the first excited state. Namely, the shorter laser wavelength should be chosen for the equilibrium internuclear distance due to the large energy difference, while the longer laser wavelength will be better for large internuclear distance. In addition, an appropriate laser intensity that is close to the multiphoton region is also essential.

IV. CONCLUSION

In conclusion, we have presented a detailed study of the electron dynamics of the LOHG in hydrogen molecular ions subject to an intense linearly polarized laser field. We find some fine subpeak structures in the low-order emitted radiation spectra at the large internuclear distances. The results calculated from the 3D TDSE are interpreted with the help of a model based on the two-level assumption. We confirm that these subpeak structures are caused by the interferences in cycles of all the multiphoton radiation emitted from the dipole transition between the ground $1\sigma_g$ and the first excited $1\sigma_u$ state within the incident laser pulse duration. Combined with the wavelet transform of the HHG, we find that the radiation spectra of the LOHG in H_2^+ with large internuclear distances is different from that with equilibrium internuclear distance. Furthermore, by investigating the harmonics generation of H_2^+ with different internuclear distances, we find that the fine subpeak structures can be observed in small internuclear distance with appropriate laser wavelength and peak intensity. In addition, we note that the position and the number of the subpeak in low-order spectra is relevant to the incident laser pulse duration. Our analysis provides insights into the detailed LOHG mechanisms.

ACKNOWLEDGMENTS

This work was supported by the National Natural Science Foundation of China (Grants No. 11465016, No. 11674268, and No. 11764038) and the Scientific Research Foundation of Physics of CPEE-NWNU, P.R. China.

[1] M. Hentschel *et al.*, Nature (London) **414**, 509 (2001).
[2] M. Drescher *et al.*, Science **291**, 1923 (2001).
[3] M. Chini, K. Zhao, and Z. Chang, Nat. Photon. **8**, 178 (2014).
[4] F. Silva, S. M. Teichmann, S. L. Cousin, M. Hemmer, and J. Biegert, Nat. Commun. **6**, 6611 (2015).
[5] S. Haessler *et al.*, Nat. Phys. **6**, 200 (2010).
[6] S. Baker *et al.*, Science **312**, 424 (2006).
[7] J. Itatani *et al.*, Nature (London) **432**, 867 (2004).
[8] R. Kienberger *et al.*, Science **297**, 1144 (2002).
[9] M. Drescher *et al.*, Nature (London) **419**, 803 (2002).
[10] J. Henkel, T. Witting, D. Fabris, M. Lein, P. L. Knight, J. W. G. Tisch, and J. P. Marangos, Phys. Rev. A **87**, 043818 (2013).
[11] E. J. Takahashi, P. F. Lan, O. D. Mucke, Y. Nabekawa, and K. Midorikawa, Nat. Commun. **4**, 2691 (2013).
[12] X. B. Bian and A. D. Bandrauk, Phys. Rev. Lett. **108**, 263003 (2012).
[13] M. Chini *et al.*, Nat. Photon. **8**, 437 (2014).
[14] F. Brizuela *et al.*, Sci. Rep. **3**, 1410 (2013).
[15] E. P. Power *et al.*, Nat. Photon. **4**, 352 (2010).
[16] D. C. Yost *et al.*, Nat. Phys. **5**, 815 (2009).
[17] J. A. Hostetter, J. L. Tate, K. J. Schafer, and M. B. Gaarde, Phys. Rev. A **82**, 023401 (2010).
[18] W. H. Xiong, J. W. Geng, J. Y. Tang, L. Y. Peng, and Q. Gong, Phys. Rev. Lett. **112**, 233001 (2014).
[19] P. C. Li, Y. L. Sheu, C. Laughlin, and S.-I. Chu, Nat. Commun. **6**, 7178 (2015).
[20] W. H. Xiong, J. Z. Jin, L. Y. Peng, and Q. H. Gong, Phys. Rev. A **96**, 023418 (2017).
[21] J. Heslar and S.-I. Chu, Sci. Rep. **6**, 37774 (2016).
[22] K. N. Avanaki, D. A. Telnov, H. Z. Jooya, and S.-I. Chu, Phys. Rev. A **92**, 063811 (2015).
[23] M. Protopapas, D. G. Lappas, C. H. Keitel, and P. L. Knight, Phys. Rev. A **53**, 2933(R) (1996).
[24] X. M. Tong and S.-I. Chu, Phys. Rev. A **61**, 021802(R) (2000).
[25] M. Abramowitz and I. A. S. C. Slater, *Handbook of Mathematical Functions* (Dover, New York, 1965).
[26] B. Zhang, J. M. Yuan, and Z. X. Zhao, Phys. Rev. A **85**, 033421 (2012).
[27] L. Tao, C. W. McCurdy, and T. N. Rescigno, Phys. Rev. A **79**, 012719 (2009); L. Malegat, P. Selles, and A. K. Kazansky, *ibid.* **60**, 3667 (1999).
[28] D. A. Telnov and S.-I. Chu, Phys. Rev. A **71**, 013408 (2005).
[29] P. Antoine, B. Piraux, and A. Maquet, Phys. Rev. A **51**, 1750(R) (1995).
[30] M. B. Gaarde, Ph. Antoine, A. L'Huillier, K. J. Schafer, and K. C. Kulander, Phys. Rev. A **57**, 4553 (1998).
[31] P. B. Corkum, Phys. Rev. Lett. **71**, 1994 (1993).
[32] I. Kawata, H. Kono, and Y. C. Fujimura, J. Chem. Phys. **110**, 11152 (1999).
[33] A. DiPiazza, E. Fiordilino, and M. H. Mittleman, Phys. Rev. A **64**, 013414 (2001).
[34] C. Figueira de Morisson Faria, Phys. Rev. A **66**, 013402 (2002).
[35] D. A. Telnov, J. Heslar, and S.-I. Chu, Phys. Rev. A **90**, 063412 (2014).
[36] X. L. Ge, T. Wang, J. Guo, and X. S. Liu, Phys. Rev. A **89**, 023424 (2014).
[37] C. Yu, N. Fu, C. Y. Dai, H. Wang, G. Z. Zhang, and J. Q. Yao, Opt. Commun. **300**, 199 (2013).